

Powder Metallurgy HIP Process Study and Mechanical Property Evaluations for IN740H

Shenyan Huang^{1*}, Timothy Hanlon¹, John Shingledecker², Ian Spinelli¹, Marija Drobnjak¹, Kevin Shoemaker¹, Cole Crawford¹

¹ GE Research, Niskayuna, NY 12309, USA

² Electric Power Research Institute, Charlotte, NC 28262, USA

*Corresponding author: huangs@ge.com

Abstract (150~200 words)

The effects of Hot Isostatic Pressing (HIP) parameters and powder size distribution (PSD) on the resulting microstructure and properties of powder metallurgy (P/M) IN740H has been investigated. Properties can be substantially tailored through the appropriate management of these parameters. Applying a thermal pre-soak to the input powder prior to the sintering stage of HIP can significantly increase average grain size and coarse grain fraction, enabling a trade for improved creep resistance at the expense of tensile strength. Powder thermal pre-soak was found to have a larger impact on microstructure and properties than the use of a coarser PSD alone. Additionally, substantial grain growth and grain boundary migration is observed in P/M IN740H at HIP temperatures above 1260°C. Given its inherently finer grain size, P/M HIP IN740H typically outperforms its cast and wrought counterpart in tensile response. Creep life at 700°C to 800°C was inferior to wrought due to PPBs coincident with grain boundaries which served as cavity nucleation sites, leading to lower creep ductility. The ability to adjust the microstructure toward a more balanced creep and tensile behavior allows P/M HIP IN740H to be considered for high-temperature applications in Advanced Ultra-supercritical Steam and supercritical carbon dioxide power cycles.

Keywords: hot isostatic pressing, powder metallurgy, superalloy, tensile, creep

1. Introduction

Advanced Ultra-supercritical Steam (AUSC) and supercritical carbon dioxide (sCO₂) power cycles both offer the potential of significantly increased efficiency for electricity generation, compared to conventional steam power cycle. Both cycles operate at temperatures above 620°C, requiring the use of γ' strengthened Ni-based superalloys to meet plant lifetime needs. Use of Ni-based superalloys, rather than steels used for lower temperature cycles, significantly increases plant costs. As a result, a levelized cost of electricity (LCoE) comparison for both advanced power cycles shows that gains from efficiency improvements are reduced by increased plant costs [1-5]. Two γ' strengthened Ni-based superalloys primarily utilized for advanced power cycles are Haynes® 282® alloy (H282) and Inconel® alloy 740H® (IN740H). As a wrought product, H282 and IN740H are the highest creep strength ASME boiler and pressure vessel code-approved Ni-based alloys with IN740H being a key AUSC material for tubing and piping with a variety of applications in high-temperature service. To date, development on both alloys for advanced power cycles has focused only on cast or wrought products where there is limited supply chain. These supply chain limitations become more restrictive the larger the component required. Further, initial attempts to cast both alloys in thick walls or complex shapes resulted in casting defects such as cracking, large porosities, and oxide inclusions, all requiring extensive weld repair [1,6]. On the other hand, machining large complex components from even larger forgings produces excessive material waste and high cost. Forging limitations inherent to the material and process can also constrain the overall component size.

Alternatively, powder metallurgy (P/M) near-net-shape (NNS) hot isostatic pressing (HIP) has been studied to reduce the manufacturing cost of large structural components in advanced power cycles [7]. In the NNS HIP process, a sacrificial steel capsule sized to the near-final shape of the component is manufactured and then filled with powder to consolidate by HIP [8,9]. This process uses 2~3X less material than the cast and wrought alternative, while still enabling complex part geometries, reducing both final machining and overall manufacturing costs. The NNS HIP

process can also reduce the number of welds in assemblies, eliminate requisite weld repairs often found complex cast geometries, improve microstructural uniformity and chemical homogeneity, and increase ultrasound inspectability due to the fine uniform grain size inherent to the process. NNS HIP manufacturing combined with weld practices developed to join P/M and wrought structures can potentially overcome the current cost and technical hurdles for many large complex-shape components in AUSC or sCO₂ turbines.

As in other P/M consolidation processes, NNS HIP of IN740H will result in a network of second phase particles that reside on prior particle boundaries (PPBs). The effect of PPB particles on mechanical behavior in powder materials has been studied for decades, with emphasis typically placed on minimization of these phases, and deformation processing to break up continuous PPB networks [10-12]. The presence of PPB particles is believed to hinder metallurgical bonding between adjacent powder particles during the sintering process. Additionally, their inherently low ductility causes planes of weakness in the material if the PPB network is not sufficiently disrupted [10]. This can lead to property debits under monotonic and cyclic loading conditions. Since the NNS HIP process typically precludes subsequent deformation processing post-HIP, careful control of these PPB particles is required to meet property requirements.

It is well known that PPB particles generate pinning forces that resist grain boundary migration. Their presence is often the controlling factor that determines grain size limits in super-solvus heat treatment schedules. Variants of the Zener pinning formula [13] have been used to successfully describe their impact on the final grain size. One version of the Zener equation is $P_s = 3F_v \gamma / 2r$, where P_s is pinning pressure, F_v is particle volume fraction, γ is the boundary energy per unit area, and r is the particle radius. In general, smaller particle sizes and higher particle fractions lead to higher pinning pressure on grain boundaries. Evolution of the PPB network largely occurs prior to sintering. Despite the high quench rates associated with gas atomization, there remains a chemical segregation within the resultant powder particles, with certain elements preferentially rejected to the inter-dendritic regions. Elements that segregate to these regions in Ni-base superalloys include Mo, Ti, Nb, Hf, and Zr. While carbides tend to form within these regions of chemical segregation, very few discrete oxides are found in the as-atomized powder particles, a testament to the industry recognition of the need to control oxygen content [14]. Despite that control, argon atomized powder generally has a nanometer scale native oxide present at the periphery of each powder particle. As the powder is thermally exposed during the consolidation process, discrete oxides begin to form prior to the onset of sintering, where it is believed the oxide forming elements, such as Hf and Zr, getter tramp oxygen from within the material and from the powder container atmosphere. Once sintering begins and open porosity transitions to closed porosity, powder particle free-surface area reduces, as does the volume of gas immediately available to these surfaces. This is where PPB particle evolution slows considerably, suggesting that the most effective means of altering its distribution is before sintering begins.

It is also well established that in both H282 and IN740H, high-temperature creep strength is sensitive to grain size [15-17]. In general, testing on these wrought alloys suggest finer grain size leads to a larger stress and temperature region where diffusional creep properties need to be considered [18]. P/M-HIP IN740H is expected to have finer grain size resulting in lower creep strength, but, as previously described, PPBs can also pin grain boundaries which may mitigate the diffusional flow in the grain boundary regions. Since rupture strength sets the allowable stresses in the time dependent regime, creep testing should be carefully selected over a range of temperatures and stresses to cover the likely mechanistic considerations and provide an understanding of the complexities of the microstructure and practical engineering application of the data.

Given that NNS HIP components will be used in the as-HIP condition without further deformation processing, the PPB network and grain size will need to be optimized to gain traction for this technology in high temperature structural components. In the present work, the effects of HIP temperature, presoak heat treatment prior to HIP, powder size distribution, and solution heat treatment temperature after HIP are investigated for IN740H, using lab-scale HIP samples. Detailed quantitative analyses of PPB particle size and fraction, as well as grain size and distribution are reported. Tensile and creep properties on select conditions are evaluated and compared to wrought IN740H properties. This work provides the initial evaluation of P/M HIP IN740H for high-temperature pressure-boundary structural applications in AUSC or sCO₂ power cycles.

2. Experimental Procedure

IN740H argon gas atomized powder was produced at the Wyman-Gordon R&D facility. The melt stock for atomization was provided by Special Metals and originated from a vacuum induction melted (VIM) and vacuum arc remelted (VAR) IN740H ingot that was subsequently extruded to pipe. The baseline powder for this study is labeled as “fine” (F) and was sieve cut to -100 mesh (powder finer than 140 μm). A small quantity of coarse powder with +100 mesh (powder coarser than 140 μm) was also obtained and is labeled “coarse” (C). Five unique PSDs were then generated by mixing the fine and coarse powders to specific weight ratios: 100% fine powder (100F), 50% fine and 50% coarse (50F-50C), 30% fine and 70% coarse (30F-70C), 10% fine and 90% coarse (10F-90C), and 100% coarse (100C). Powder mixing/blending was conducted by tumbling end over end in a container for minutes. The actual powder size distribution (PSD) was measured using a Microtrac S3500. Oxygen level in the powder samples was quantified using a LECO ONH 836 Oxygen/Nitrogen/Hydrogen Analyzer.

Lab-scale HIP cans were prepared for microstructure and property evaluations. All HIP cans were evacuated and outgassed at elevated temperature, then helium leak checked prior to consolidation. The temperature and pressure in all HIP cycles were controlled with the same linear ramp rates. All cans were subjected to a HIP cycle of 15ksi for 4 hours, with HIP temperatures intentionally varied from cycle to cycle. The density of the fully consolidated IN740H was measured by the Archimedes method.

Detailed microstructure analysis was performed for the PSDs and HIP conditions listed in Table 1. A transverse slice of each HIP can was prepared for microstructure analysis. High resolution backscattered electron imaging was taken on a Hitachi SU-70 FEG-SEM with Bruker XFlash 6 60mm² SDD EDS detector to reveal the grain structure and secondary phases. Backscattered electron images were acquired with a BSE solid state diode (PDBSE) detector. Both secondary electron and backscattered electron images were obtained over a range of magnifications. Due to the small size and scarcity of PPB particles, 20 random locations were selected and imaged at 5000x under high resolution backscattered mode to achieve a total of ~200 PPB particles with statistical representation. These images were analyzed to quantify the size, number density, and area fraction of PPB particles. To quantify grain size distribution, Electron Backscatter Diffraction (EBSD) was performed on a Hitachi SU-70 FEG-SEM with an Oxford Aztec Symmetry EBSD detector at accelerating voltage of 20 kV. Step size was 250nm. Scan area was 1000 x 750 μm , which covered more than 1000 grains. 10° grain boundary maps excluding $\Sigma 3$ twin boundaries were used to generate grain size distribution plots.

Tensile and creep tests were conducted on select conditions. Solution and age heat treatments were applied after HIP to allow more direct comparison with wrought IN740 in the fully heat treated state. Several samples were subjected to the typical wrought IN740 solution and 1-step age heat treatment, while others were subjected to higher solution temperatures. The combinations of PSD, HIP condition, and heat treatment for which mechanical properties were evaluated are summarized as follows:

- 1) Baseline: -100 mesh powder, 1204°C/15ksi/4hr HIP, 1121°C/1hr solution followed by water quench (WQ), 800°C/4hr aging followed by air cool (AC); this solution and aging condition is typical of wrought IN740;
- 2) Higher HIP temperature: -100 mesh powder, 1227°C/15ksi/4hr HIP, 1121°C/1hr/WQ solution, 800°C/4hr/AC aging;
- 3) Higher solution temperature:
 - 3a) -100 mesh powder, 1204°C/15ksi/4hr HIP, 1204°C/1hr/WQ solution, 800°C/4hr/AC aging;
 - 3b) -100 mesh powder, 1204°C/15ksi/4hr HIP, 1232°C/1hr/WQ solution, 800°C/4hr/AC aging;
- 4) Higher HIP temperature and higher solution temperature: -100 mesh powder, 1227°C/15ksi/4hr HIP, 1232°C/1hr/WQ solution, 800°C/4hr/AC aging;
- 5) Presoak T4/t4: -100 mesh powder, presoak T4/t4 heat treatment, 1204°C/15ksi/4hr HIP, 1121°C/1hr/WQ solution, 800°C/4hr/AC aging;
- 6) PSD Evaluation: 30F-70C powder, 1204°C/15ksi/4hr HIP, 1121°C/1hr/WQ solution, 800°C/4hr/AC aging.

Tensile tests were performed on a servo-hydraulic MTS load frame at various temperatures (room temperature, 700°C, 760°C, and 815°C). The test temperatures of 700°C and 760°C are within the range of desired AUSC and sCO₂ turbine and component operating temperatures. Each specimen measured 50.8mm total length, 19.05mm gauge length, and 3.56mm gauge diameter. All tests were conducted in displacement control at a crosshead speed of 0.5mm per minute to failure, with an extensometer applied to measure strain passively. Creep-rupture tests were conducted in Applied Test Systems (ATS) lever-arm type creep frames in accordance with ASTM E139 on standard round bars with a gauge diameter of 6.35mm and a gauge length of either 25.4mm or 31.8mm at temperatures of 700°C, 750°C, and 800°C and stresses ranging from 110 to 325MPa. Extensometers were attached to the sample shoulders to measure creep strain accumulation. Post-test examinations were conducted by using wire electro discharge machining (EDM) to split the sample in half along the axis followed by standard metallographic mounting and polishing procedures prior to optical and SEM analysis.

3. Results and Discussion

3.1 Phases and PPB particles in P/M HIP IN740H

Table 2 compares the as-received IN740H powder chemistry to the target and limits of wrought IN740H/IN740, showing that the powder chemistry is within the composition limits. The powder contains low oxygen (62 ppm) and nitrogen (59 ppm), as a result of using stock material with low interstitials and careful powder handling in inert environment. The theoretical density was assumed to be the same as the fully consolidated material, which was measured to be 8.158 g/cm³. An absolute tap density of 5.48 g/cm³ or a relative tap density of 67.2% was obtained for the IN740H powder.

The equilibrium phases of the as-received powder chemistry as a function of temperature are predicted using the Thermo-Calc TTNi7 database. As shown in Figure 1, the solvus of the γ' phase is around 983°C. All the studied HIP temperatures are above the γ' solvus temperature, thus γ' does not play a role in the resulting grain size post-HIP. A variety of minor phases are calculated to be present at high temperatures. Nb- and Ti-rich MC type carbides are calculated to be stable in the temperature range of 714°C ~ 1317°C. Ti-rich carbonitride and alumina (aluminum oxide) are also stable throughout the temperature range. Extremely low amounts of Ti-rich borides are also predicted in the temperature range of 804°C ~ 1037°C, although they were not observed by high-resolution SEM imaging. Similarly, Sigma and Eta phases are predicted but not observed. This is expected as numerous studies have not observed sigma in IN740H and eta phase, when stable, generally only forms after long-term thermal aging or creep [16,19,20]. Cr-rich M₂₃C₆ type carbide is shown to be stable below 806°C. Therefore, MC carbides, Ti-rich carbonitrides, and alumina are the minor phases most relevant to the studied HIP window.

Figure 2a presents the typical as-HIP IN740H microstructure of the baseline condition. In the backscattered electron image, discrete particles with dark contrast are observed to decorate the PPBs. The PPBs also align with grain boundaries, indicating their propensity to effectively restrict grain boundary migration. Figures 2b and 2c represent higher magnification views of the same area under (b) backscattered and (c) secondary electron imaging modes. The corresponding EDS maps from the location represented in Figures 2b and 2c are displayed in Figure 2d. Two types of PPB particles are observed in P/M HIP IN740H:

- Nb- and Ti-rich carbide/carbonitrides, which are dark in contrast in the backscattered image and grey in contrast in the secondary image.
- Alumina, which is dark in contrast in the backscattered image and bright in contrast in the secondary image.

PPB carbides have higher number density and fraction than PPB oxides. The presence of these PPB particles is consistent with the Thermo-Calc predictions.

3.2 Effect of HIP Temperature

The effect of HIP temperature on the grain structure is depicted in Figure 3. When HIP temperature increases from 1121°C to 1204°C, a coarser grain size and lower fraction of smaller grains are observed. Further increasing HIP

temperature from 1204°C to 1227°C did not produce a measurable difference, whereas 1260°C and 1299°C HIP conditions show substantial grain growth. The average grain sizes measured using the mean intercept length method for HIP temperatures of 1204°C, 1260°C, and 1299°C are 18.5µm, 25.7µm, and 34.4µm, respectively. When the HIP temperature is below 1260°C, almost all grain boundaries align with the PPBs, indicating the strong drag force exerted by the PPB particles. When the HIP temperature is above 1260°C, large fractions of grain boundaries are found to migrate beyond the PPB particles. Note that 1299°C is close to the MC carbide solvus temperature of 1317°C. Lower fraction of MC carbides is predicted at 1299°C (Figure 1b). It is likely that both thermal driving force and some dissolution of MC carbides at high HIP temperatures have contributed to lower the barrier for grain boundary migration, promoting significant grain growth. It should be noted that high HIP temperature has the risk of boride liquation related property degradation, which was not fully studied in the present work. In addition, commercial HIP units for large components are readily available at HIP temperatures below 1227°C, while the capacity becomes rare for HIP temperatures above 1260°C, especially at the large component sizes of the AUSC turbine. In the present study, 1204°C HIP was selected as the baseline condition and adopted in the processing studies and mechanical property evaluations.

3.3 Effect of Thermal Presoak Heat Treatment

In general, smaller PPB particle sizes and larger volume fractions lead to higher pinning pressure on grain boundaries, restricting grain growth. Thermally presoaking the powder prior to HIP effectively coarsens the PPB particles, reducing this pinning effect and generating coarser grains post-consolidation. Two presoak temperatures and four presoak times (total 8 conditions) are reported here. The grain size distributions analyzed by EBSD are plotted in Figure 4. Data suggest that higher presoak temperatures and longer presoak times yield coarser grain sizes (manifested by lower fraction of fine grains and higher fraction of coarse grains) and wider grain size distribution. For comparison, the mean intercept length of the presoak T4/t4 condition is 32.3µm versus 18.5µm in the baseline condition with no thermal presoak. The results for PPB particle diameter and area fraction are plotted together with grain size in Figure 5, where the data points represent average values and error bars represent standard deviation among the analyzed particles. No distinction between carbides and alumina is made when quantifying PPB dimensional and area fraction characteristics through image analysis. Figure 5 shows that PPB particle size also increases with longer presoak time and higher presoak temperature, while PPB particle fraction remains constant. The average particle diameter measured 134nm in the baseline condition with no thermal presoak, versus 213nm in the T4/t4 presoak condition. This is indicative of the PPB particle coarsening that occurs during the presoak heat treatment.

3.4 Effect of Powder Size Distribution

In general, larger powder particles have a lower surface to volume ratio than fines, leading to reduced adsorbed oxygen and lower volume fractions of native oxide, reducing the number density of PPB particles post-HIP. Therefore, controlling powder size distribution can be an effective method for PPB and grain size control. Various PSDs were sampled in this study to evaluate this effect (Figure 6a). Figure 6b shows the resulting grain size distributions post-HIP, which shift to larger grain sizes with increased fraction of coarse powder. However, relative to the thermal presoak T4/t4 condition, all the PSD variants maintained a much larger fraction of fine grains and fewer coarse grains, resulting in a smaller shift in the average grain size. Figure 5 suggests that coarser powder generates larger PPB particle sizes. This may result from the micro-segregation differences in coarse vs fine powder, due to the local solidification rate differences between the two particle sizes. Additional segregation of Ti and Nb in coarser particles could promote more substantial carbide formation and growth. Although PPB particle size differences were measured vs PSD, their area fraction in each variant was comparable to the baseline, in line with expectation.

3.5 Correlation between PPB Particles and Grain Size

Figure 5 summarizes the trends observed between PPB particle characteristics and grain size, over the range of materials and processing conditions studied. The PPB particle area fraction is relatively restricted to 0.4% ~ 0.8%, across all conditions. Given the measurement error, it is assumed that the conditions evaluated in this study did not impact the overall area or volume fraction of these particles. The PPB particle diameter does correlate with grain size, consistent with the Zener pinning theory. Powder blending to coarser PSDs was not as effective as the presoak heat

treatment at coarsening PPB particles and therefore did not impact grain size to the same degree. PPB particle size of the 1299°C HIP condition seems to be an outlier and off the trend, which is not clearly understood at the moment. Alternative way to directly compare grain size distribution is the cumulative frequency plot displayed in Figure 5(c). Curve shifting to the right side indicates a reduced fraction of fine grains and an increased fraction of coarse grains, consistent with larger average grain size. The curves in the order from right to left are presoak T4, presoak T3, PSD powder blending and 1260°C HIP, baseline condition, confirming the efficacy of presoak T4/t4 in coarsening grain size. Presoak T4 and T3 conditions do have overlapping region indicating that similar grain size distribution may be generated at either lower temperature longer time or higher temperature shorter time of presoak. The cumulative frequency of 1299°C HIP is in proximity with presoak T4 shorter time and T3 longer time. In comparison, the cumulative frequency of a lower HIP temperature 1260°C appears to be comparable with [30F-70C] and [10F-90C] PSDs, with finer grain size than presoak T3 conditions. 1227°C HIP and the baseline HIP do not show obvious difference.

3.6 Tensile Properties

The yield strength, ultimate tensile strength (UTS), and elongation to failure for select P/M HIP conditions are provided in Figure 7, with wrought IN740H data shown for comparison. The baseline HIP condition has a slightly higher yield strength and comparable UTS to wrought IN740H. Conditions with a) higher HIP temperature (1227°C HIP + 1121°C solution) and b) higher HIP temperature and higher solution temperature (1227°C HIP + 1232°C solution) show similar yield strength and UTS behavior to the baseline. Presoak T4/t4 and PSD 30F-70C conditions show lower yield strength than baseline, but still comparable to wrought IN740H. The grain coarsening in these conditions leads to reduced Hall-Petch strengthening, relative to the finer grained baseline. PSD 30F-70C also has a lower UTS at 700°C and 760°C than other HIP conditions and wrought IN740H. In terms of tensile elongation, the baseline condition shows lower ductility than wrought IN740H. Presoak T4/t4 has comparable elongation at 700°C as wrought IN740H, while there is a small debit at room temperature. PSD 30F-70C has comparable ductility at room temperature as wrought IN740H, but lower ductility at 700°C and 760°C. Metallography of the longitudinal cross section in the tensile fracture location reveals that failure occurred predominantly along the PPBs, reinforcing the need to better control the network of PPB particles in as-HIP microstructures.

3.7 Creep Evaluation

Creep-rupture tests were conducted on four different combinations of HIP and post-HIP heat-treatments as follows:

- **Baseline:** -100 mesh powder, 1204°C/15ksi/4hr HIP, 1121°C/1hr solution followed by water quench (WQ), 800°C/4hr aging followed by air cool (AC)
- **Higher HIP temperature:** -100 mesh powder, 1227°C/15ksi/4hr HIP, 1121°C/1hr/WQ solution, 800°C/4hr/AC aging including samples taken from an industrial produced component [7]
- **Higher HIP temperature and higher solution temperature:** -100 mesh powder, 1227°C/15ksi/4hr HIP, 1232°C/1hr/WQ solution, 800°C/4hr/AC aging
- **Presoak T4/t4:** -100 mesh powder, presoak T4/t4 heat treatment, 1204°C/15ksi/4hr HIP, 1121°C/1hr/WQ solution, 800°C/4hr/AC aging

While the higher solution temperature of 1232°C was not included in the detailed EBSD study of grain size distribution, the average grain size measured on the sample was equivalent to the results on the effect of HIP temperature in Section 3.2 which show no significant difference in grain size in comparison to the 1121°C temperature.

Creep-rupture test conditions were selected based on the author's experience to produce rupture times greater than 300 hours as past research on wrought IN740H shows this is sufficient duration to make initial predictions for longer-term behavior of interest to advanced energy system conditions [16]. In total, 14 tests totaling over 12,000 hours of testing time including multiple tests exceeding 2,000 hours were completed for this evaluation. Figure 8 shows the time to rupture results and rupture ductility (elongation and reduction of area) in comparison to the wrought IN740H averages (solid line) and ductility range (dashed line) from Ref. [16]. Inspection of the graph shows that none of the P/M-HIP met the expected wrought average rupture life. Analysis of the rupture results show the baseline condition was approximately -40% on a stress basis below the wrought creep performance. The slightly higher HIP temperature of 1227°C has minimal effect on improving the creep performance. The addition of a higher solution annealing

temperature may improve the creep strength, but it is still -35% compared to wrought performance based on two datapoints. In contrast, the presoak condition dramatically improves rupture life in general doubling the life compared to other tested conditions at all testing temperatures. This results in a debit of ~-25% compared to wrought. Overall, creep ductility was near or below wrought minimum values with increasing ductility as temperature increases. No significant differences were observed for the different conditions, which suggests the presoak condition is likely not changing the failure mode of the tests.

To further understand the microstructural features contributing to failures, Figure 9 shows both dark and light field optical metallography of failed samples. The use of dark field imaging allows for identification of PPBs without etching while the unetched light field images only show creep cavities. Creep cavitation and microcracking are observed throughout the sample gauge at grain boundaries coincident with the PPBs. Overall size and distribution of the PPBs was similar between all samples. The SEM image in Figure 10 provides a higher magnification image of typical creep cavitation observed in the P/M-HIP IN740H. Creep cavities and extensive creep cracking is observed along PPBs normal to the applied stress but grain boundaries within the prior particles do not show any damage. Overall, the post-test microstructural observations support the mechanical data where PPBs are controlling rupture ductility, which doesn't change significantly with the different HIP and heat-treatment conditions, but increasing grain size using pre-soaking conditions can achieve rupture strength ~ - 25% from mean IN740H wrought behavior. While the high-temperature tensile data of all the samples met minimum requirements, the creep tests clearly showed a differentiation in behavior. Most importantly, the creep results show the pinning effect of PPBs on grain growth is a significant factor in limiting the high-temperature performance of P/M-HIP IN740H where higher HIP and/or solution annealing temperatures have minimal effect on changing the creep-rupture strength of the alloy. Conversely, the use of pre-soaking to coarsen the PPB carbide and oxide networks allows for grain growth which results in improved creep properties. Longer-term experiments on one pre-soak condition to ~2,000 hours show that there is still likely room for optimization and further creep strength improvement through a combination of pre-soaking and optimization of the HIP and solution annealing cycle.

4. Conclusions

As-HIP Ni-base superalloys such as IN740H generally have a finer grain structure and reduced creep capability relative to their cast and wrought counterparts. Coarsening the grain size of this material is one method to recover a portion of the creep debit. The effects of powder thermal presoak, powder size distribution, HIP temperature, and solution heat treat temperature on PPB structure and resulting grain size were investigated using lab-scale HIP samples of IN740H. Presoak heat treatment prior to HIP was shown to effectively coarsen PPB particles and shift average grain size from 18 μm to 32 μm . While coarser powder size distributions demonstrated a minor effect on grain size, PSD alone was deemed less effective at coarsening grain size, relative to presoak. Substantial grain growth and grain boundary migration is observed with HIP temperatures above 1260°C. Yield strength and ultimate tensile strength of P/M HIP conditions are comparable or higher than wrought IN740H, with the exception of the coarse PSD condition. A small debit in tensile ductility is observed for all the studied conditions, an effect driven by the nature of the PPB particle network. Creep-rupture strength was significantly less than wrought properties. The best performing condition was the pre-soak condition which resulted in rupture lives of approximately -25% below mean (stress basis). Inspection of the ductility data and post-test rupture metallographic characterization shows the PPBs coincident with grain boundaries lead to lower rupture ductility in all samples. Further improvements in creep appear possible from a combination of higher HIP temperatures (beyond typical industrial equipment studied here) and processing methods to minimize PPBs. With an allowance for thicker component wall sections to compensate for creep debits observed, P/M HIP IN740H shows promise for high-temperature applications in Advanced Ultra-supercritical Steam and supercritical carbon dioxide power cycles.

Acknowledgment

This work was funded by US Department of Energy, Office of Fossil Energy, under award number DE-FE0031818 with Program Manager Vito Cedro. Yali Su and Chris Perlee at GE Research are acknowledged for LECO analysis and powder HIP preparation. Beth Lewis and Andrew Marshall at Wyman-Gordon are acknowledged for providing high quality IN740H powder. The authors would like to thank technical discussion and collaboration with Victor

Samarov, Alex Bissikalov at Synertech PM Inc., Jack deBarbadillo at Special Metals, Jason Mortzheim at GE Research, and Alex Bridges at EPRI.

Conflict of Interest

The authors declare that they have no conflict of interest.

References

- [1] J. Moore, DOE Final report for DE-EE0005804, “Development of a High Efficiency Hot Gas Turboexpander and Low-Cost Heat Exchangers for Optimized CSP Supercritical CO₂ Operation” (2019) <https://doi.org/10.2172/1560368>
- [2] DOE funded project DE-FE0028979, Supercritical Transformational Electric Power. <https://netl.doe.gov/carbon-management/sco2/step10pilotplant>
- [3] E.J. Parker, J.P. Shingledecker, J. Siefert, Advanced in Materials technology for Fossil Power Plants: Proceedings from the 8th International Conference, Albufeira, Algarve, Portugal, 11-14 October 2016 (ASM International, Ohio, 2016).
- [4] H.L. Hendrix, “Advantages of A-USC for CO₂ capture in Pulverized Coal Units”, Advances in Materials Technology for Fossil Power Plants: Proceedings from the 7th International Conference, Waikoloa, Hawaii, USA, 22-25 October 2013 (ASM International, Ohio, 2014).
- [5] R. Purgert, J.P. Shingledecker, D. Saha, M. Thangirala, G. Booras, J. Powers, H. Hendrix, “Materials for advanced ultrasupercritical steam turbines”, 2015. <https://doi.org/10.2172/1243058>.
- [6] P.J. Maziasz, High Temperature Mechanical Properties and Microstructure of Cast Ni-Based Superalloys for Steam Turbine Casting Applications, 6th International Conference on Advances in Materials Technology for Fossil Power Plants, Santa Fe, New Mexico, 31 August – 3 September, 2010.
- [7] S. Huang, J. Mortzheim, V. Samarov, J.P. Shingledecker, J. deBarbadillo, R. Gollihue, M. Soare, B. Lewis, T. Hanlon, “Low Cost HIP Fabrication of Advanced Power Cycle Components and PM/Wrought Inconel 740H Weld Development - Final Technical Report”, 2021, <https://doi.org/10.2172/1822264>.
- [8] C. Bampton, W. Goodin, T. Van Daam, G. Creeger, S. James, Net-shape HIP powder metallurgy components for rocket engines, Proceeding of International Conference of Hot Isostatic Pressing, Paris, France, 22-25 May, 2005.
- [9] V. Samarov, D. Seliverstov, E. Khomyakov, A. Bissikalov, D. Gandy, L. Loubier, D. Novotnak, HIP of large scale PM components for nuclear power generation, Advances in Powder Metallurgy and Particulate Materials – Proceeding of the 2015 International Conference on Powder Metallurgy and Particulate Materials, PowderMet 2015, San Diego, CA, USA, 17-20 May 2015.
- [10] D.R. Chang, D.D. Krueger, R.A. Sprague, Superalloy Powder Processing, Properties and Turbine Disk Applications, Superalloys 1984, Proceedings of the Fifth International Symposium on Superalloys, Warrendale, PA, USA, pp. 245-273, 7-11 October 1984.
- [11] R. Thamburay, A.K. Koul, W. Wallace, M.C. de Malherbe, Prior Particle Boundary Precipitation in PM Superalloys, Modern Developments in Powder Metallurgy, Proceedings of the 1984 International Powder Metallurgy Conference, Princeton NJ 17-22 June 1984 (Volumes 15-17 of Modern developments in powder metallurgy, pp. 635-673).
- [12] N.G. Ingesten, R. Warren, L. Winberg, The Nature and Origin of Previous Particle Boundary Precipitates in PM Superalloys, High Temperature Alloys for Gas Turbines 1982, ed. R. Brunetaud, D. Coutsouradis, T.B. Gibbons, Y. Lindblom, D.B. Meadowcroft, R. Stickler, (Springer, Dordrecht, 1982), p. 103.
- [13] C.S. Smith, *Trans. AIME*, 175, 15(1948).
- [14] G.A. Rao, M. Srinivas, D.S. Sarma, *Mater. Sci. Eng., A*, 435-436, 84(2006). <https://doi.org/10.1016/j.msea.2006.07.053>
- [15] M.L. Santella, P.F. Tortorelli, M. Render, B. Pint, H. Wang, V. Cedro III, X. Chen, *Mater. Sci. Eng., A*, 838, 142785(2022). <https://doi.org/10.1016/j.msea.2022.142785>
- [16] J.P. Shingledecker, N.D. Evans, G.M. Pharr, Influences of composition and grain size on creep-rupture behavior of Inconel alloy 740, *Mater. Sci. Eng., A*, 578,277(2013). <https://doi.org/10.1016/j.msea.2013.04.087>

- [17] J.P. Shingledecker, E. Griscom, A. Bridges, J. deBarbadillo, B. Baker, Effect of Processing on the Microstructure and Creep Performance of INCONEL® Alloy 740H® Sheet, The 7th International Supercritical CO2 Power Cycles Symposium. San Antonio, Texas, USA, 21-24 February 2022.
- [18] M. Soare, C. Shen, V. Cedro III, Modeling creep of Ni-base superalloys for applications in advanced ultra-supercritical power generation, Proceedings of the 14th International Symposium on Superalloys, ed. S. Tin, M. Hardy, J. Clews, J. Cormier, Q. Feng, J. Marcin, C. O'Brien, A. Suzuki, (Springer Nature, Cham Switzerland, 2020), p. 702. https://doi.org/10.1007/978-3-030-51834-9_68
- [19] K.A. Unocic, J.P. Shingledecker, P.F. Tortorelli, *JOM*, 66, 2535-2542 (2014). <https://doi.org/10.1007/s11837-014-1208-4>
- [20] N.D. Evans, P.J. Maziasz, R.W. Swindeman, G.D. Smith, *Scr. Mater.*, 51,503, (2004). <https://doi.org/10.1016/j.scriptamat.2004.05.047>

Table 1: Detailed microstructure analysis was performed for the following PSDs and HIP conditions.

PSD	Thermal Presoak Conditions	HIP Conditions
-100 mesh powder	No Presoak prior to HIP	1204°C/15ksi/4hr
-100 mesh powder	Presoak at one of two temperatures (T4>T3) and one of four times (t4 > t3 > t2 > t1)	1204°C/15ksi/4hr
[50F-50C], [30F-70C], [10F-90C], [100C]	No Presoak prior to HIP	1204°C/15ksi/4hr
-100 mesh powder	No Presoak prior to HIP	15ksi/4hr at one of five temperatures: 1121°C, 1149°C, 1227°C, 1260°C, 1299°C

Table 2: Actual composition of the IN740H powder in the present study compared to nominal composition of wrought IN740H and its upper/lower limits (in weight percent, wt.%).

	Wrought IN740H, nominal	Wrought IN740H, Min	Wrought IN740H, Max	IN740H argon gas atomized powder
Ni	bal.	bal.	bal.	bal.
Cr	24.5	23.5	25.5	24.6
Co	20	15	22	20.2
Al	1.35	0.2	2	1.34
Ti	1.35	0.5	2.5	1.34
Nb	1.5	0.5	2.5	1.5
C	0.03	0.005	0.08	0.039
Mo	0.1	-	2	0.06
Si	0.15	-	1	0.15
Fe	-	-	3	0.2
Mn	-	-	1	0.2
Cu	-	-	0.5	0.01
P	-	-	0.03	0.004
S	-	-	0.03	0.0009
B	-	0.0006	0.006	0.001
O	-	-	-	0.0062
N	-	-	-	0.0059

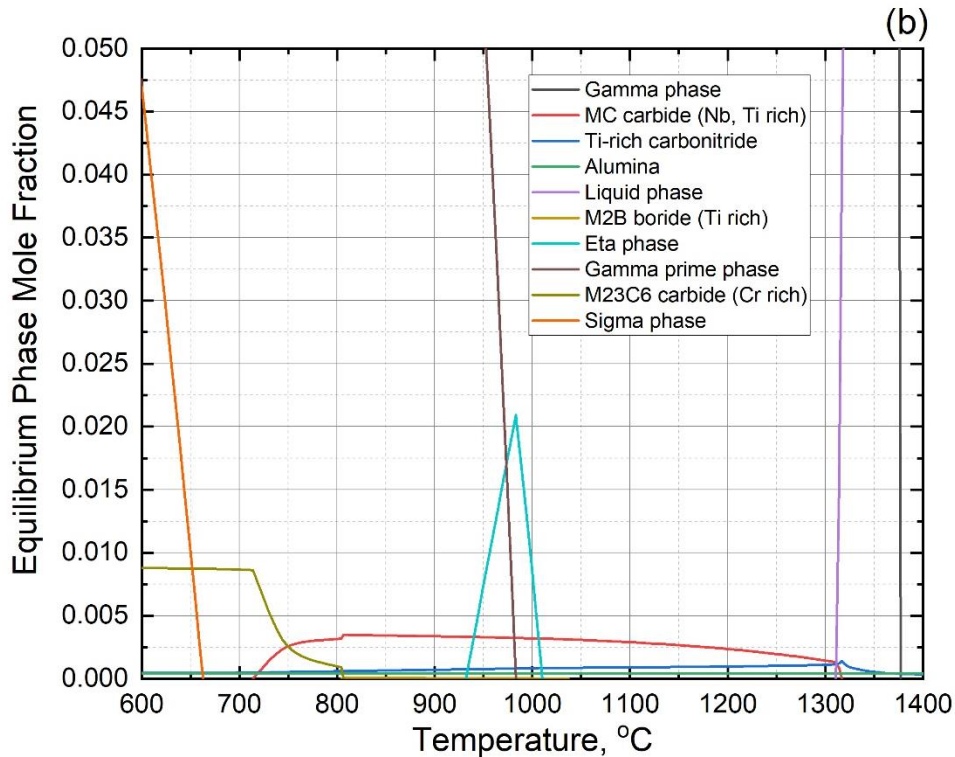
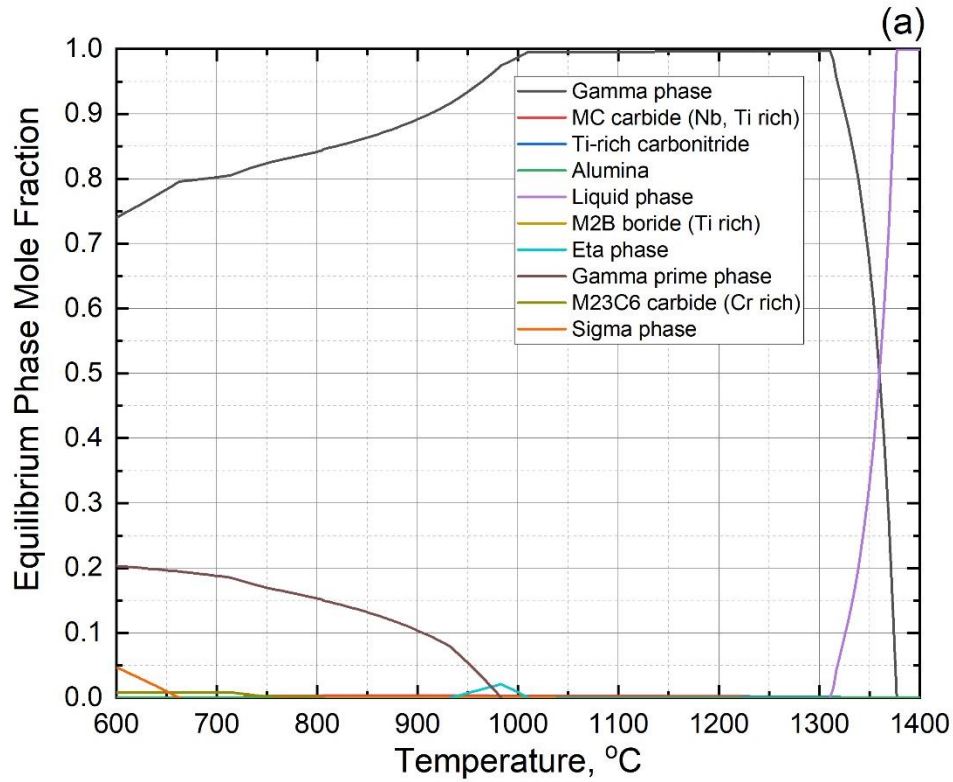


Figure 1: Thermo-Calc equilibrium calculation of (a) phase mole fraction vs. temperature for the as-received IN740H powder chemistry using the TTNi7 database and (b) an enlarged view of the minor phases from (a).

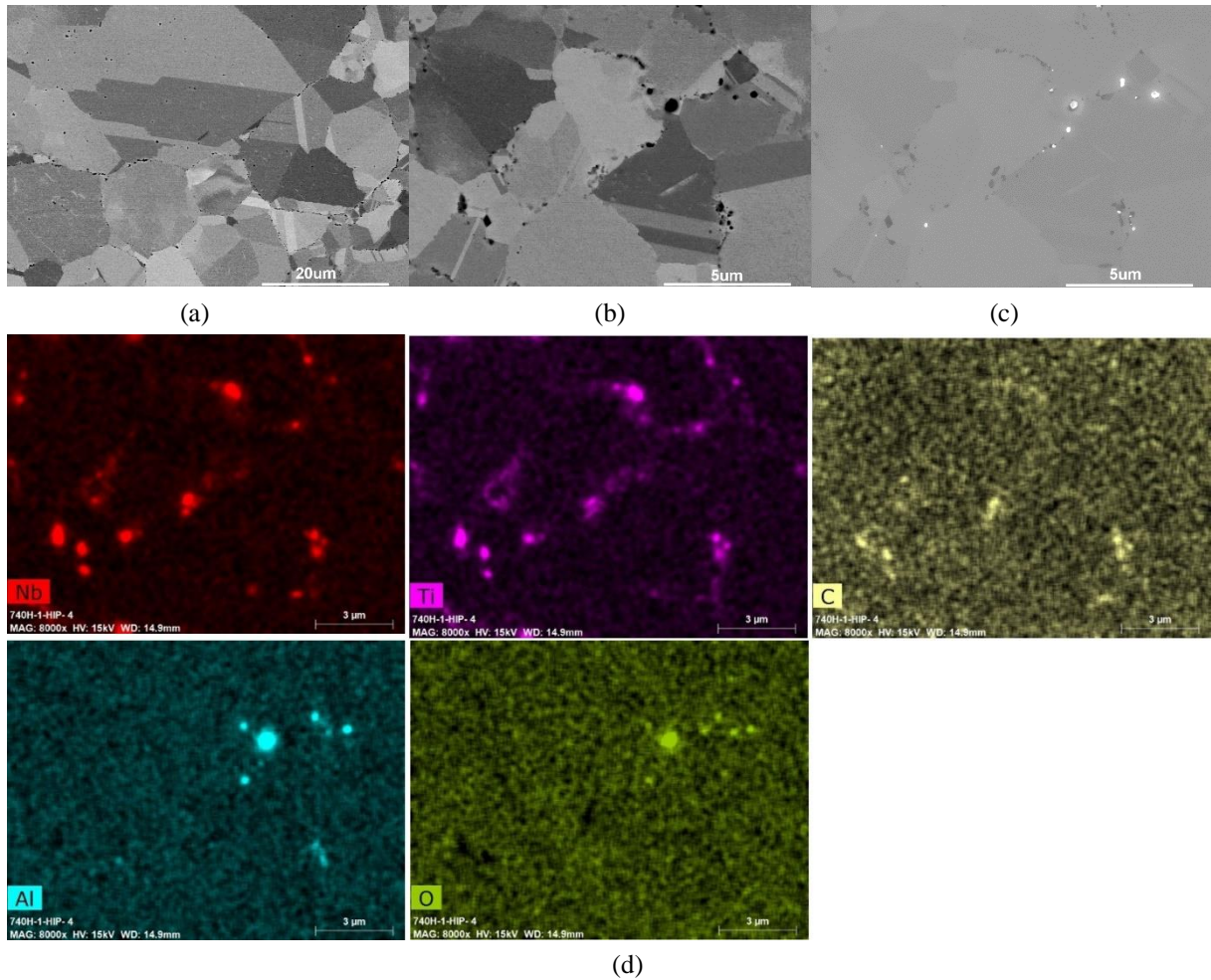


Figure 2: (a-b) Backscattered electron images of the baseline IN740H material, HIP'd at 1204°C/15ksi/4hr. (c) Secondary electron image at the same field of view as (b). (d) corresponding EDS maps from the same field of view as (b-c), highlighting the chemistry of the PPB particles.

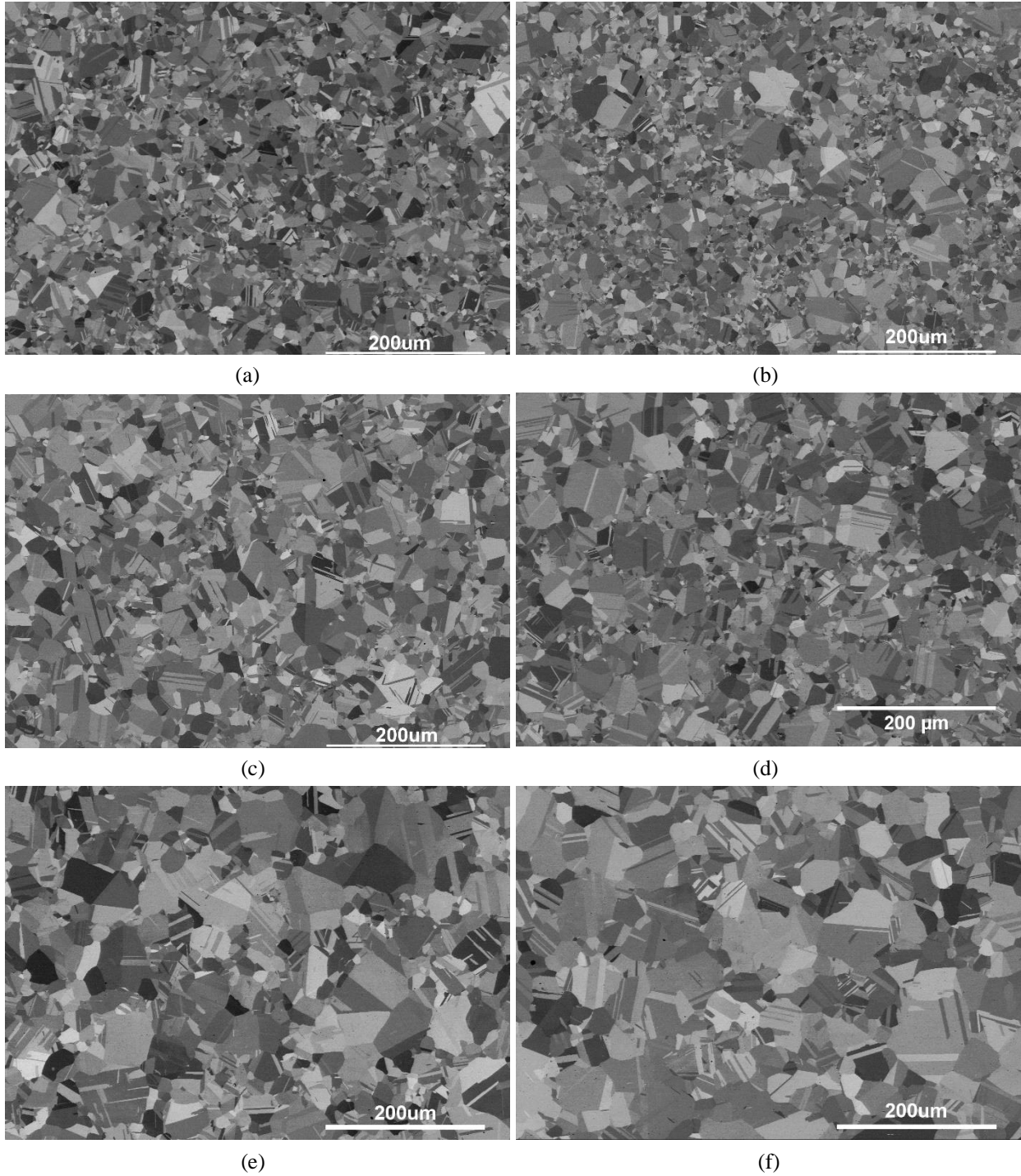


Figure 3: Backscattered electron images of IN740H powder HIP processed at (a) 1121°C, (b) 1149°C, (c) 1204°C, (d) 1227°C, (e) 1260°C, (f) 1299°C.

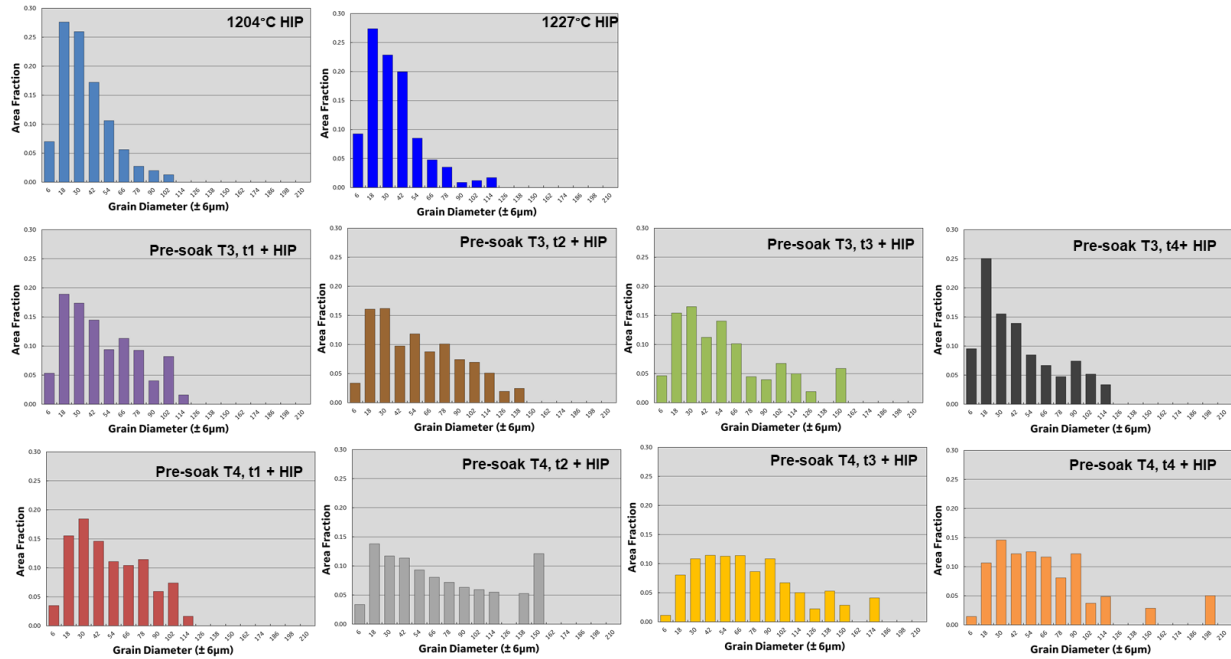
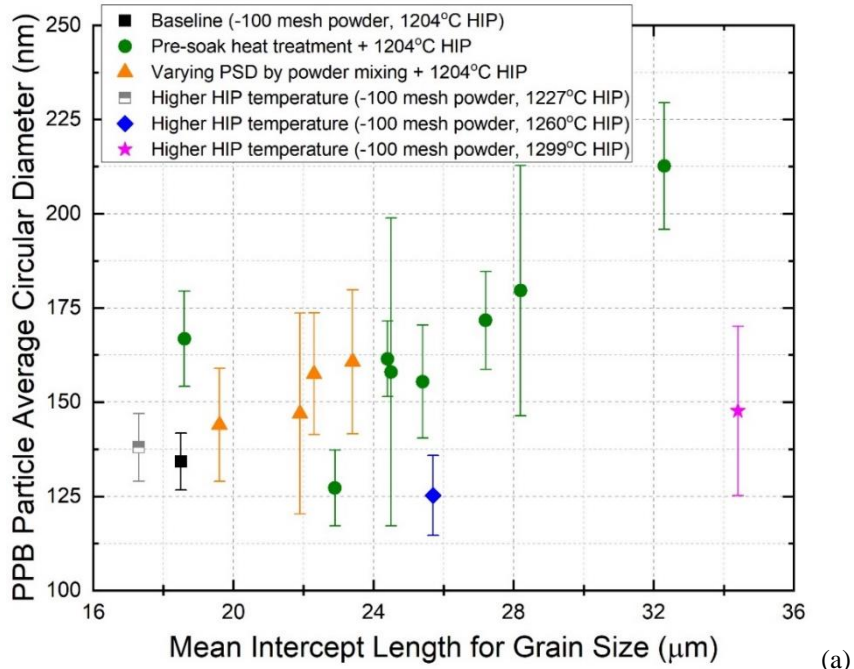
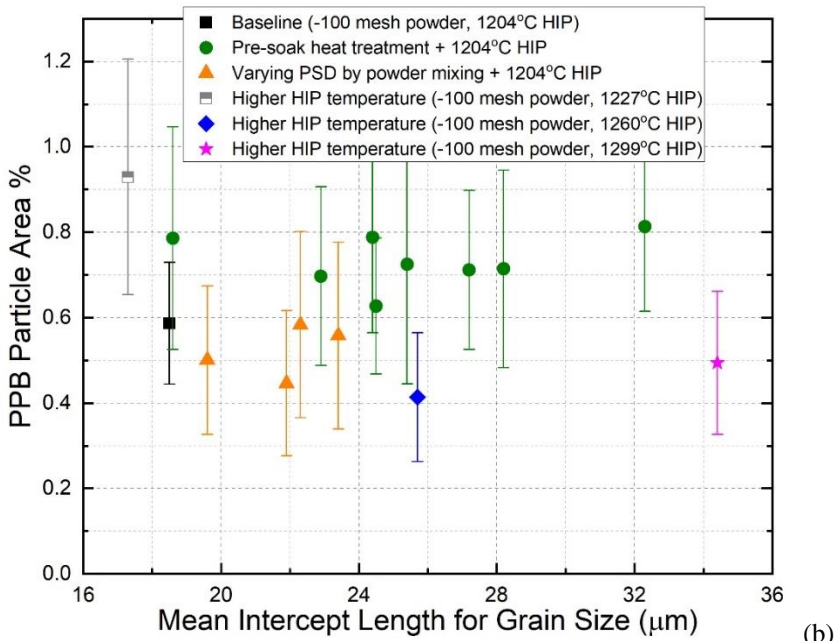


Figure 4: Grain size distributions quantified using EBSD 10° grain boundary maps for the baseline HIP and eight pre-soak + HIP conditions evaluated.



(a)



(b)

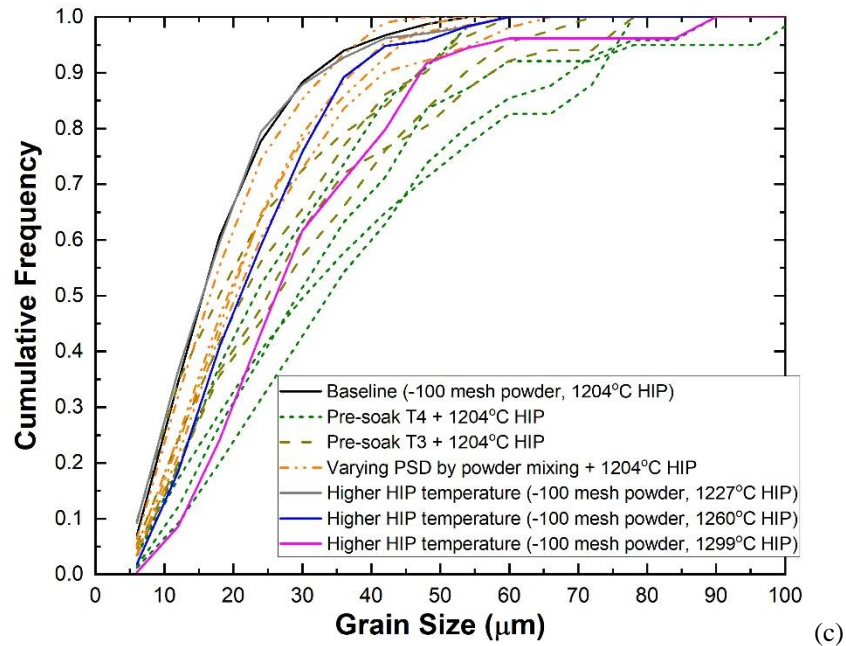
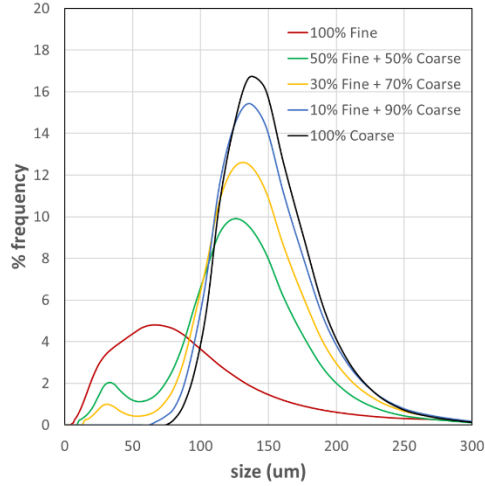
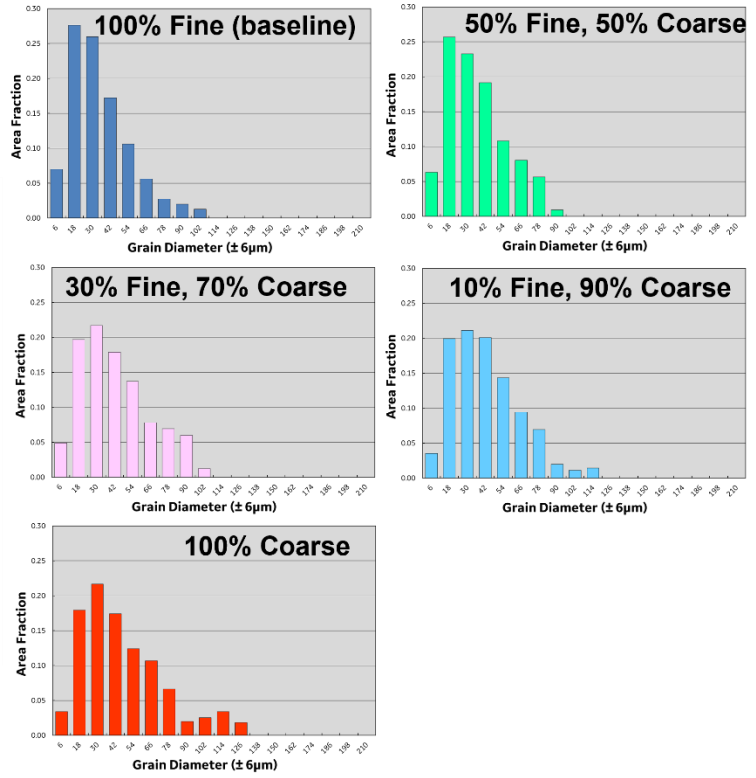


Figure 5: (a) PPB particle average circular diameter vs. mean intercept length grain size. (b) PPB particle area % vs. mean intercept length grain size. (c) Cumulative frequency of grain size observed in the various HIP conditions.



(a)



(b)

Figure 6: (a) PSDs on powder particle volume basis generated at various mixtures of -100 mesh (fine) and +100 mesh (coarse) powder. (b) Resulting grain size distribution quantified using EBSD 10° grain boundary maps.

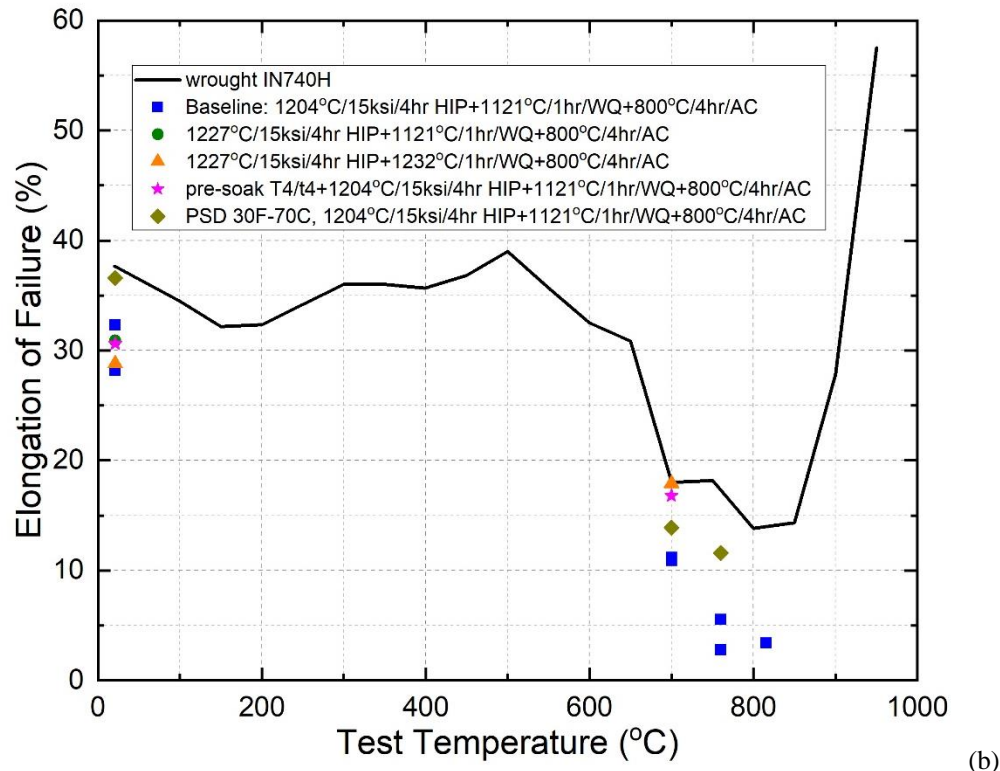
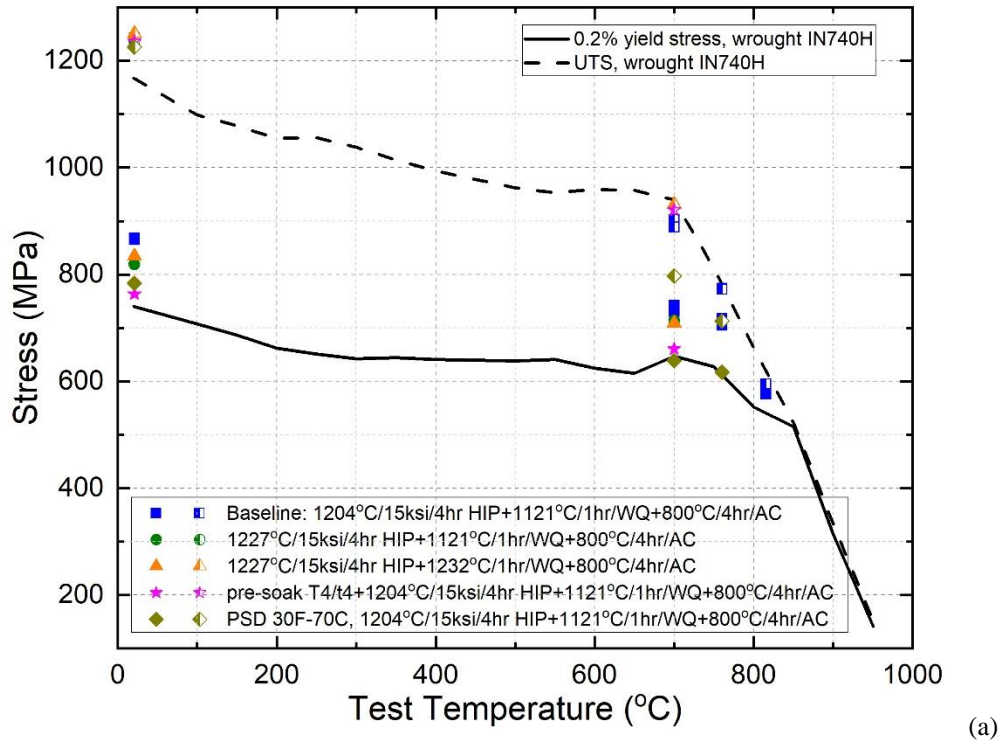


Figure 7: (a) 0.2% offset yield strength (closed symbols) and UTS (half open symbols) as a function of temperature for wrought IN740H and various P/M HIP IN740H conditions. (b) Elongation to failure for the same material conditions.

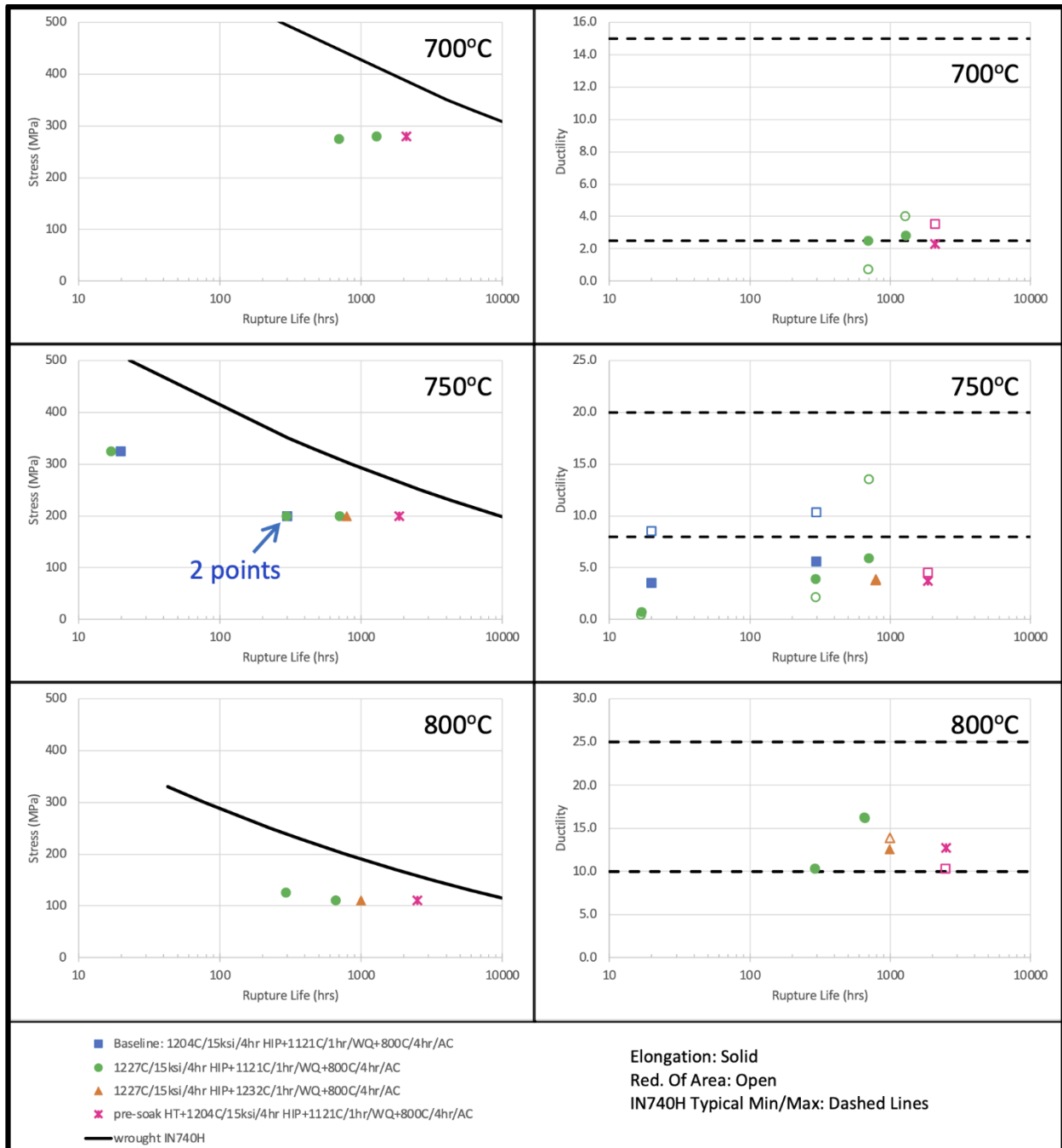


Figure 8: Time-to-rupture (left) and rupture ductility (right) results for creep testing at 700°C, 750°C, and 800°C for P/M HIP IN740H compared to average wrought behavior (solid line) and typical wrought ductility (dashed lines). Wrought IN740H data are adapted from equations and Larson-Miller plots in Ref.[16].

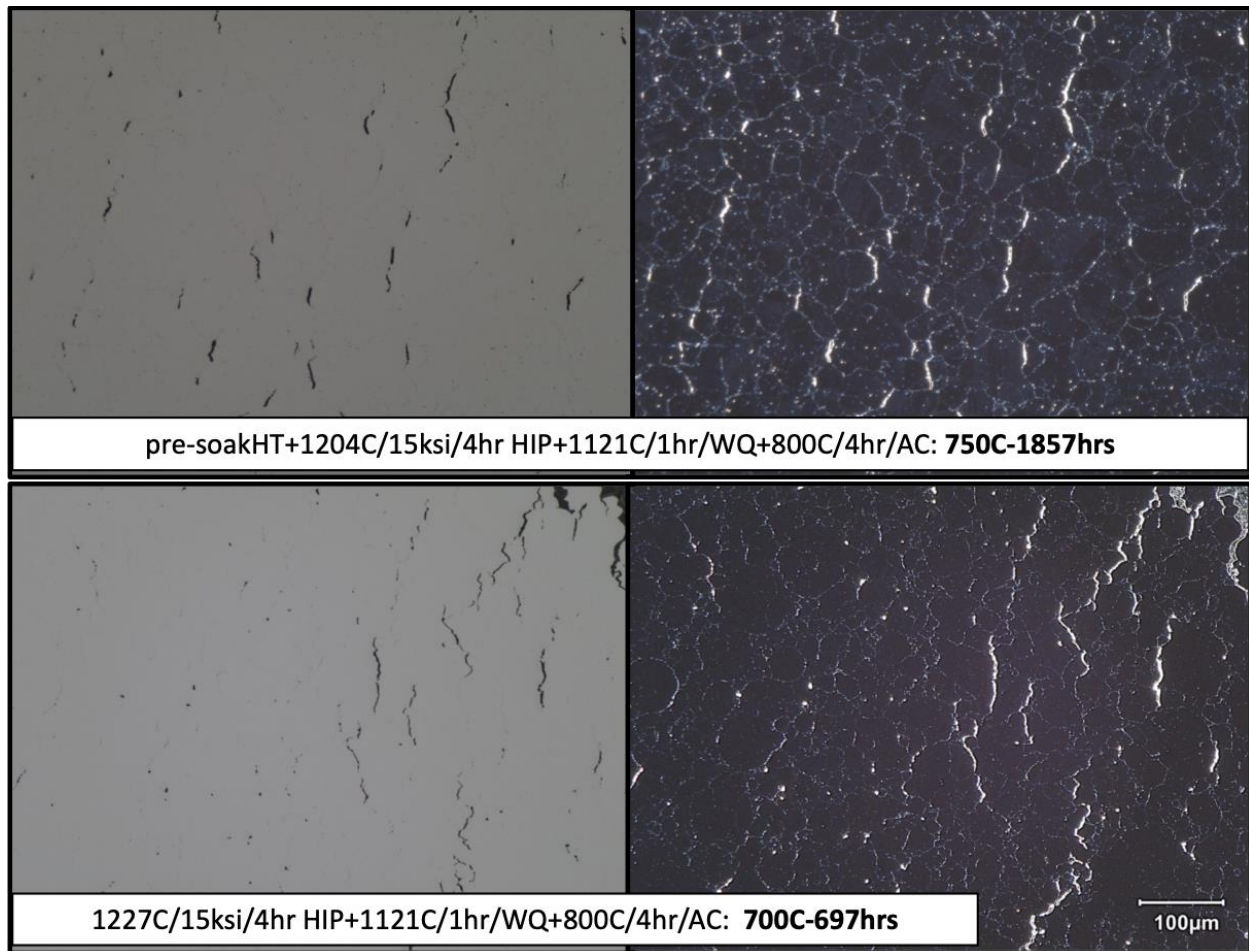


Figure 9: Creep damage (light optical left) and PPBs w/damage (dark field optical right) for pre-soak (top) higher HIP temperature (bottom) after creep testing. Stress loading direction is to the right and left of the page.

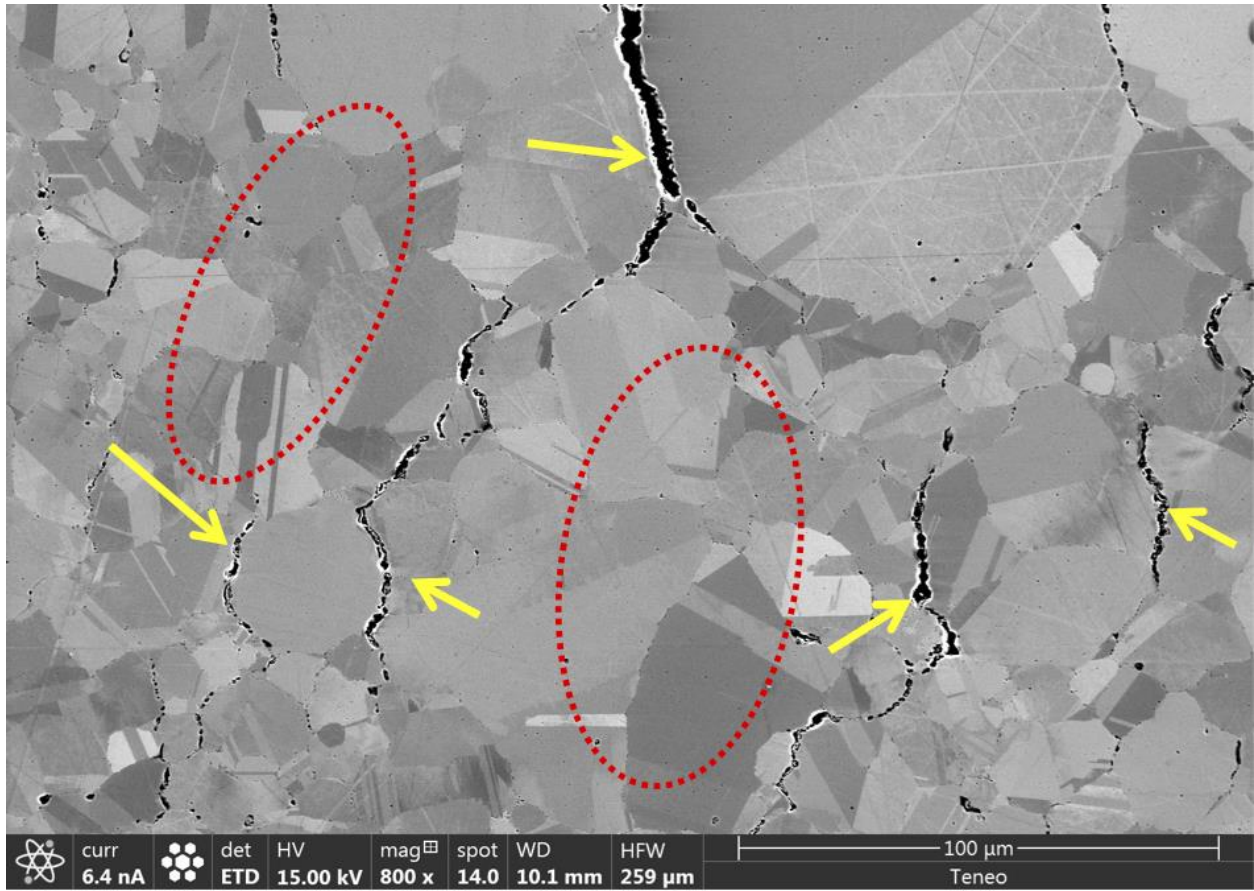


Figure 10: SEM BSE image for higher HIP temperature (1227°C/15ksi/4hr HIP, 1121°C/1hr/WQ solution, 800°C/4hr/AC) after creep testing at 750°C-200MPa for 295hrs. Yellow arrows indicate creep damage at PPBs coincident with grain boundaries and red circles indicate grain boundaries normal to applied stress which do not show creep cavitation.